Supplementary Material

The Role of Solvent Charge Donation in the Stabilization of Metal Ions in Aqueous Solution

Daniel Koch, Sergei Manzhos[1]

Department of Mechanical Engineering, National University of Singapore, 9 Engineering Drive 1, Singapore 117576, Singapore

Computational Methods

Calculations on molecules and atoms were performed using the computational chemistry program package GAUSSIAN 16.[1] The PBE0 hybrid functional by Adamo and Barone with 25% exact exchange[2, 3] was used together with Dunning's correlation consistent polarized valence triple-zeta basis set[4-8] (*cc*-pVTZ) for the comparative calculations of transition metal (TM) and non-TM complexes as well as the water molecule (ions) and hydronium ion. The PBE0 hybrid functional was found to reproduce wave function-based post-Hartree Fock results best at reasonable computational cost (see the following section *Method Tests* in the Supplementary Material), while the Bader charges and O-H stretch frequencies were found to be well-converged at the triple-zeta basis set level (see following section *Basis Set Test* in the Supplementary Material). The integral equation formalism variant of the polarizable continuum model[9-11] (IEFPCM) as implemented in GAUSSIAN 16 was used

[1] Author to whom correspondence should be addressed. E-mail: mpemanzh@nus.edu.sg . Tel: +65 6516 4605; fax: +65 6779 1459.

to simulate the influence of outer water solvation shells and disordered solvent. For all calculations performed in this work, the unrestricted schemes of the corresponding methods were employed to ensure the comparability of the results.[12, 13]

The structures of the metal aquo complexes were relaxed via a Berny algorithm using an energy-represented direct inversion in the iterative subspace[14] (GEDIIS) with a convergence threshold on forces of $2 \cdot 10^{-6}$ E_h/a_0. The $[M(H_2O)_6]^{n+}$ (*M* = V, Mn, Fe, Cr, Li, Be, Al) complexes were initialized in T_H symmetry as well as in a distorted configuration of C_1 symmetry to scan along larger parts of the potential energy surface. Grid-based Bader charge analyses as implemented in the BADER v.0.95a code[15-18] were performed on respective cubes with resolutions of approximately 900 pts/a_0^3 (approx. 9.5 pts/a_0 in each principal direction), which was found to be well-converged (see following section *Bader Grid Test* in Supplementary Material). The formation energy E_f of the $[M(H_2O)_6]^{n+}$ complexes was computed as energy difference between the solvated complex ion and a M^{n+} ion in the gas phase (vacuum) plus six solvated water molecules:

$$E_f([M(H_2O)_6]^{n+}) = E\left([M(H_2O)_6]^{n+}_{(aq)}\right) - \left(E(M^{n+}_{vac}) + 6E\left(H_2O_{(aq)}\right)\right) \quad . \qquad (1)$$

All graphs in the main text and Supplementary Material were made with the program GNUPLOT version 5.2.[19]

Method Tests

Since post-Hartree Fock (HF[20-22]) methods like Møller-Plesset perturbation theory to the second order[23-28] (MP2) and coupled-cluster singles and doubles[29-32] (CCSD) scale as $O(N^5)$ and $O(N^6)$, respectively, while DFT hybrid functionals at least maintain an $O(N^4)$ scaling, it is desirable to utilize a sufficiently accurate DFT functional for geometry relaxations, computation of vibrational frequencies and Bader charge analyses. While the difference in scaling between hybrid DFT and MP2 does not seem to be overwhelming, the use of a sufficiently converged basis sets quickly makes post-

HF calculations unfeasible for the type of analysis done within this work. In order to find an appropriate DFT functional, tests on vanadium complexes were performed. First, the charge density remainders on the V center in different $[V(H_2O)_6]^{n+}$ complexes with n = 1,…,5 were compared among DFT and post-HF methods, namely the generalized-gradient approximation (GGA) functional PBE,[33, 34] the hybrid functionals PBE0[2, 3] and B3LYP,[35-37] as well as MP2 and CCSD. The results are shown in Fig. S1. For Bader charge analyses with MP2 and CCSD, the generalized densities corresponding to second-order and coupled-cluster energies, respectively, were used. All calculations were performed with the correlation consistent polarized valence double-zeta basis set by Dunning[4-8] (*cc*-pVDZ) and within the IEFPCM. The densities were generated in single-point calculations, due to the high cost of CCSD structure relaxations, using the corresponding PBE0 minimum energy geometry for all methods.

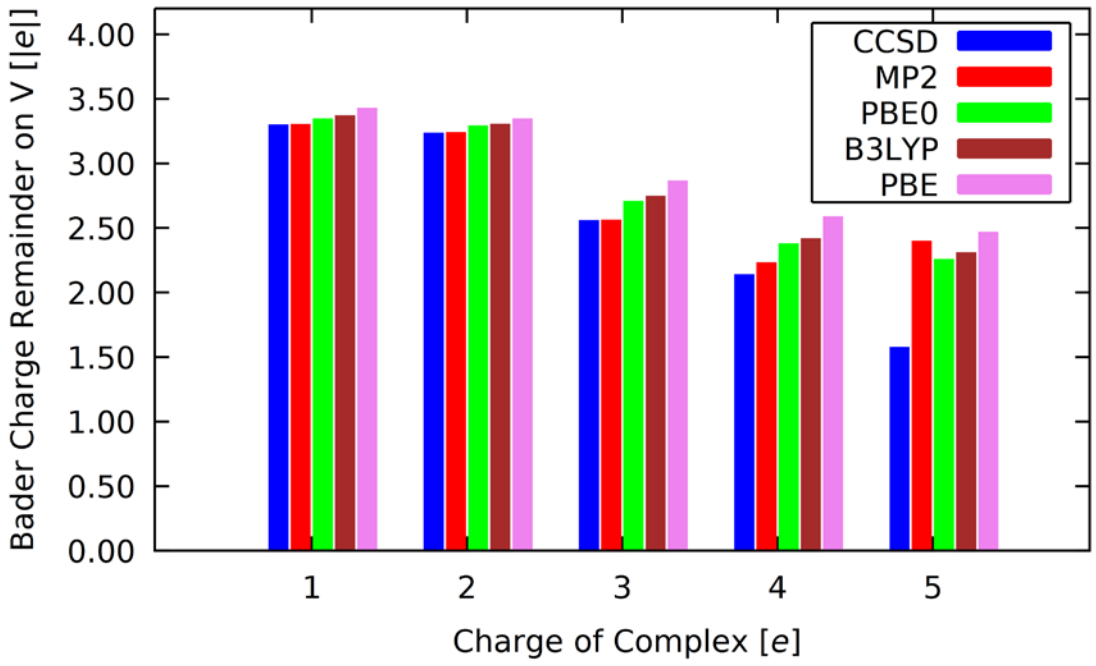

FIG. S1. Bader charge remainder on the V center for different charges n of the $[V(H_2O)_6]^{n+}$ complexes and with different methods: CCSD (blue), MP2 (red), PBE0 (green), B3LYP (brown), PBE (violet).

The deviations of MP2, B3LYP and PBE minimum energy geometry at this basis set precision do not exceed 2% on interatomic distances and angles, a range which was found to cause only negligible

changes of the central ion Bader charge.

As can be seen in Fig. S1, PBE0 in general delivers Bader charge results closest to the post-HF benchmarks. Besides Bader charges, vibrational frequencies, specifically, O-H stretch frequencies are of concern in this investigation. In Fig. S2, plots of H_2O ligand Bader charges versus average O-H stretch frequencies (after structure relaxation) as obtained with HF, MP2, PBE, B3LYP, and PBE0 and a *cc*-pVDZ basis set/IEFPCM are compared. For these tests, MP2 was used as the benchmark due to a high cost of CCSD.

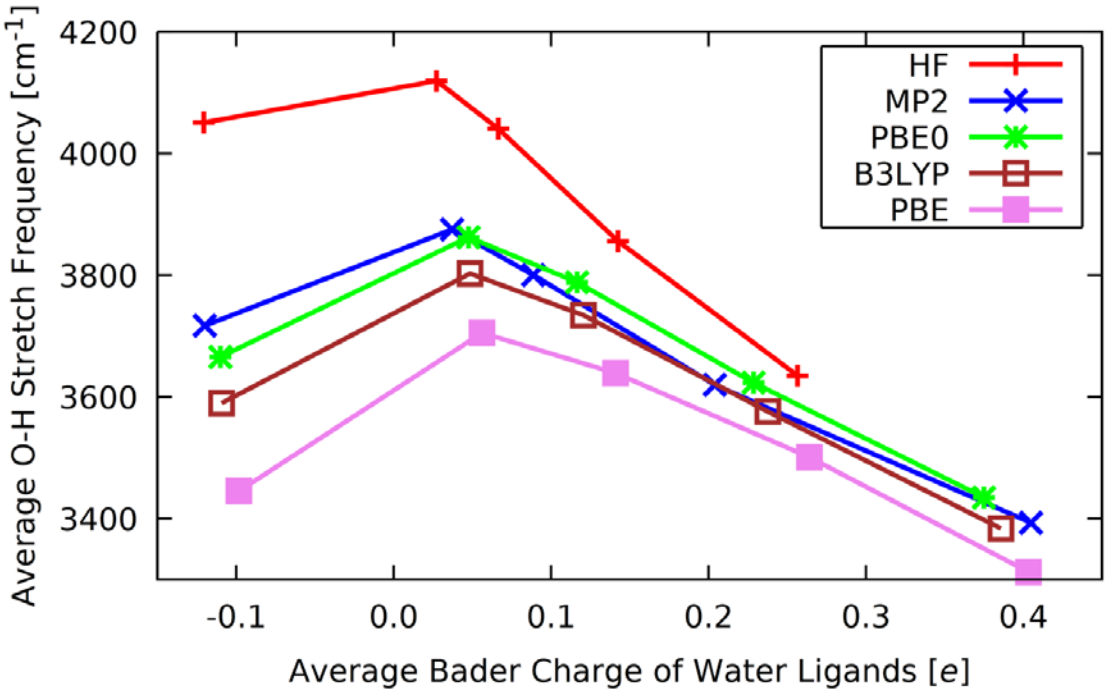

FIG. S2. Average O-H stretch frequency versus average Bader charge of the water ligands in $[V(H_2O)_6]^{n+}$ complexes with n=1...5 using different methods: HF (red, crosses), MP2 (blue, tilted crosses), PBE0 (green, asterisks), B3LYP (brown, empty squares), PBE (violet, filled squares). Increasing charges of the complexes cause an increasing Bader charge on the water ligand, i.e. n is increasing from left to right for each method.

The largest deviations from the MP2 benchmark can be observed with HF, significantly overestimating O-H stretch frequencies, while underestimating the charge transfer from the water

ligands to the transition metal ion. The PBE GGA functional on the other hand underestimates the O-H bond strength and overestimates the charge transfer. Admixture of exact exchange largely corrects for the GGA deviation, leading to a good agreement between MP2 and PBE0/B3LYP values, with PBE0 having the smaller deviations on average.

Basis Set Test

In Fig. S3 the Bader charge remainder on the metal center and the average O-H stretch frequencies (symmetric and asymmetric) of the six water ligands in relaxed $[V(H_2O)_6]^{3+}$ complexes is plotted against the size of the employed *cc*-pV*n*Z basis set[4-8] (where half-integer values denote the corresponding augmented basis sets).

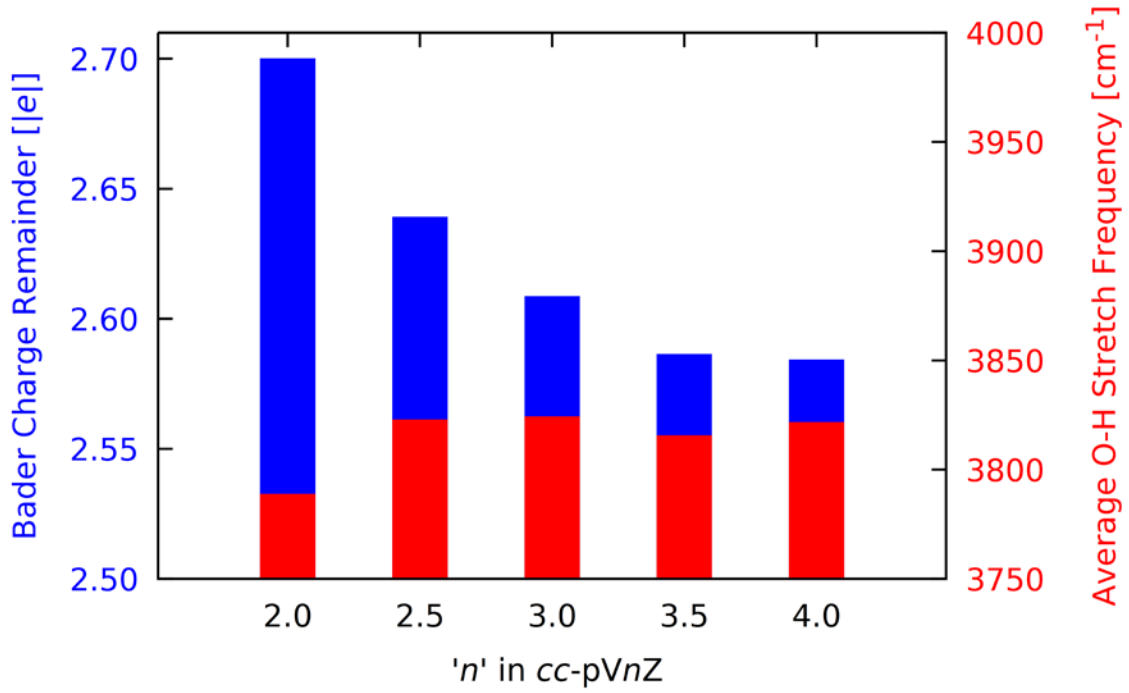

FIG. S3. Bader charge remainder (blue, left axis) on V in $[V(H_2O)_6]^{3+}$ and average O-H stretch frequencies of the water ligands (red, right axis) in dependence of the chosen basis set. The index *n* denotes the size of the *cc*-pV*n*Z basis set, with *n*=2.0 corresponding to *cc*-pVDZ, n=3.0 to *cc*-pVTZ, n=4.0 to *cc*-pVQZ, and half-integer numbers to the augmented basis sets (aug-*cc*-pVDZ and aug-*cc*-pVTZ).

Calculations were carried out with PBE0 and the IEFPCM model as described in the section *Computational Methods* above. The $[V(H_2O)_6]^{3+}$ complex was chosen as a model system for the basis set comparison, since it is a well-studied, observable complex, which occurs in aqueous V(III) solutions. As can be seen from Fig. S3, the relative differences among the results obtained with basis sets with $n>2$ are significantly smaller than the differences to *cc*-pVDZ. Since this investigation is dealing mainly with cationic complexes, the inclusion of diffuse functions seems not justified, and *cc*-pVTZ was chosen as reasonably converged basis set for the computations described in the main text.

Bader Grid Test

In order to ensure a sufficient precision of the grid-based Bader charge analysis, its dependence on the resolution of the underlying electron density was investigated. Fig. S4 shows the Bader charge remainder versus resolution (in points per cubic Bohr) of the corresponding density data for a $[V(H_2O)_6]^{3+}$ complex with PBE0/*cc*-pVTZ and IEFPCM.

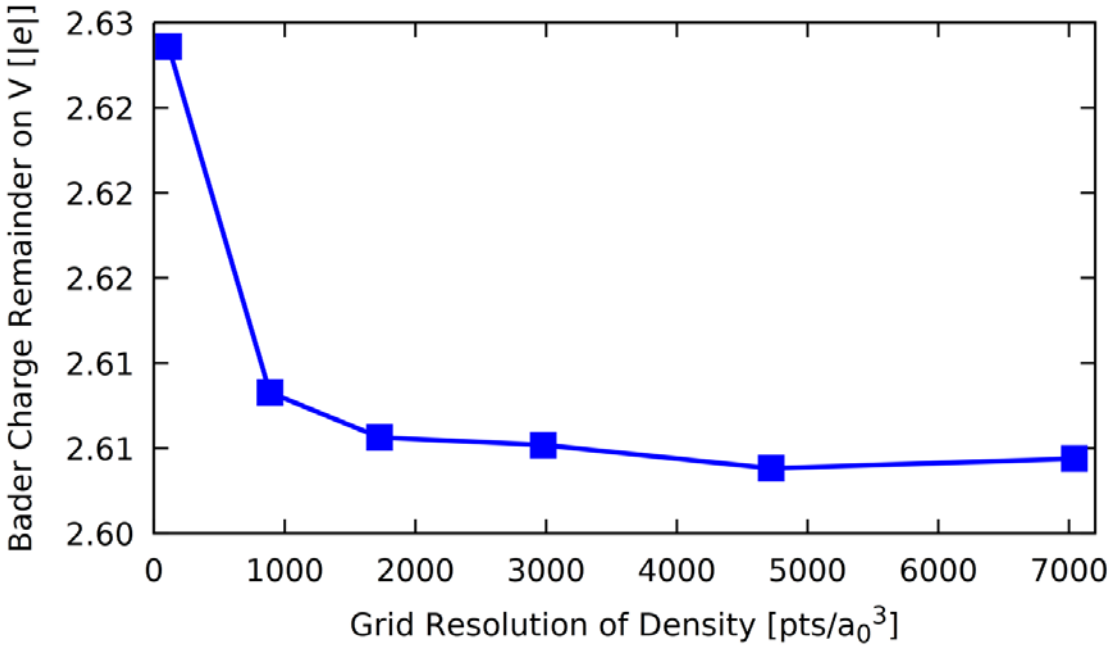

FIG. S4. Bader charge remainder on V in the $[V(H_2O)_6]^{3+}$ complex versus the resolution (points per cubic Bohr) of the electronic density used to determine the Bader charges of the atoms.

Convergence occurs quickly and the resulting Bader charge remainder does not change significantly for resolutions finer than ~900 pts/a_0^3, which was deemed a reliable choice in this investigation.

Polarizable Continuum Model Versus Vacuum

For the purpose of estimating the influence of the IEFPCM on the results and to ensure that the introduced perturbation by the solvent does not influence the overall conclusion of this investigation by unreasonably large distortions, the O-H stretch frequencies versus H_2O Bader charges for different $[V(H_2O)_6]^{n+}$ complexes with n = 1,…,5 were compared between vacuum and within the IEFPCM, as reported in Fig. S5.

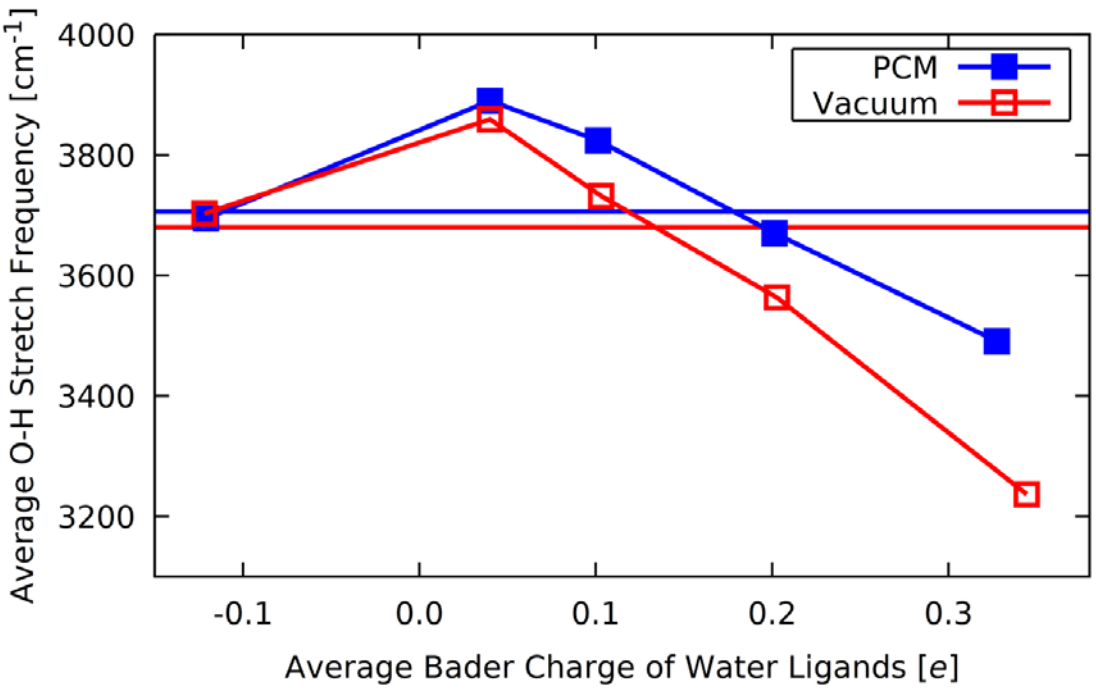

FIG. S5. Average O-H stretch frequency versus average Bader charge of the water ligands in $[V(H_2O)_6]^{n+}$ complexes with n=1...5 using a polarizable continuum model (PCM; blue, filled squares) and in vacuum (red, empty squares). Increasing charges of the complexes cause an increasing Bader charge on the water ligand, i.e. n is increasing from left to right in each case. The average O-H stretch frequency of the H_3O^+ cation in PCM (blue) and vacuum (red) are indicated by horizontal lines.

While the occurring deviations are small for hexaaqua vanadium(I) and vanadium(II) complexes, frequencies for higher oxidation states deviate up to 7% from each other and Bader charges up to 5%. However, comparison with the average O-H stretch frequency of the H_3O^+ hydronium ion reveals that in both cases the average O-H stretch frequencies for V(IV) and V(V) complexes fall below this value (see red and blue horizontal lines in Fig. S5), while for V(II) and V(III) complexes the O-H bonds are stronger than in the hydronium ion. In the vacuum case, the average stretch frequency for the V(I) complex is also slightly higher than the one for the hydronium ion, with a deviation of roughly 30 cm^{-1} (0.6%), while introducing the IEFPCM destabilizes the O-H bonds on average and lowers the ligands stretch frequencies below the one of the hydronium ion.

Spin Distributions in Hexaaqua M(II) and M(III) complexes

TABLE SI. Magnetic moments of metal center and water ligands in the investigated hexaaqua M(II) and M(III) complexes (*M* = V, Mn, Fe, Cr). All numbers given in μ_B.

Complex	**Magnetic moment of metal [μ_B]**	**Magnetic moment of solvation shell [μ_B]**
$[V(H_2O)_6]^{2+}$	+2.93	+0.07
$[V(H_2O)_6]^{3+}$	+1.95	+0.05
$[Mn(H_2O)_6]^{2+}$	+3.81	+0.19
$[Mn(H_2O)_6]^{3+}$	+4.42	+0.58
$[Fe(H_2O)_6]^{2+}$	+3.93	+0.07
$[Fe(H_2O)_6]^{3+}$	+2.90	+0.10
$[Cr(H_2O)_6]^{2+}$	+4.82	+0.18
$[Cr(H_2O)_6]^{3+}$	+3.78	+0.22

To evaluate the distribution of spin magnetic moments between metal and solvation shell, a Bader

charge analysis of the spin density of all the investigated $[M(H_2O)_6]^{2+}$ and $[M(H_2O)_6]^{3+}$ complexes (*M* = V, Mn, Fe, Cr) was performed. The results are listed in Table S1.

References

1. M.J. Frisch, G.W. Trucks, H.B. Schlegel, G.E. Scuseria, M.A. Robb, J.R. Cheeseman, G. Scalmani, V. Barone, G.A. Petersson, H. Nakatsuji, X. Li, M. Caricato, A.V. Marenich, J. Bloino, B.G. Janesko, R. Gomperts, B. Mennucci, H.P. Hratchian, J.V. Ortiz, A.F. Izmaylov, J.L. Sonnenberg, Williams, F. Ding, F. Lipparini, F. Egidi, J. Goings, B. Peng, A. Petrone, T. Henderson, D. Ranasinghe, V.G. Zakrzewski, J. Gao, N. Rega, G. Zheng, W. Liang, M. Hada, M. Ehara, K. Toyota, R. Fukuda, J. Hasegawa, M. Ishida, T. Nakajima, Y. Honda, O. Kitao, H. Nakai, T. Vreven, K. Throssell, J.A. Montgomery Jr., J.E. Peralta, F. Ogliaro, M.J. Bearpark, J.J. Heyd, E.N. Brothers, K.N. Kudin, V.N. Staroverov, T.A. Keith, R. Kobayashi, J. Normand, K. Raghavachari, A.P. Rendell, J.C. Burant, S.S. Iyengar, J. Tomasi, M. Cossi, J.M. Millam, M. Klene, C. Adamo, R. Cammi, J.W. Ochterski, R.L. Martin, K. Morokuma, O. Farkas, J.B. Foresman and D.J. Fox: Gaussian 16 Rev. B.01, (Wallingford, CT, 2016).
2. C. Adamo and V. Barone: Toward reliable density functional methods without adjustable parameters: The PBE0 model. *J. Chem. Phys.* **110**, 6158 (1999).
3. J.P. Perdew, M. Ernzerhof and K. Burke: Rationale for mixing exact exchange with density functional approximations. *J. Chem. Phys.* **105**, 9982 (1996).
4. T.H. Dunning: Gaussian basis sets for use in correlated molecular calculations. I. The atoms boron through neon and hydrogen. *J. Chem. Phys.* **90**, 1007 (1989).
5. R.A. Kendall, T.H. Dunning and R.J. Harrison: Electron affinities of the first-row atoms revisited. Systematic basis sets and wave functions. *J. Chem. Phys.* **96**, 6796 (1992).
6. K.A. Peterson, D.E. Woon and T.H. Dunning: Benchmark calculations with correlated molecular wave functions. IV. The classical barrier height of the $H+H_2 \rightarrow H_2+H$ reaction. *J.*

Chem. Phys. **100**, 7410 (1994).

7. A.K. Wilson, T. van Mourik and T.H. Dunning: Gaussian basis sets for use in correlated molecular calculations. VI. Sextuple zeta correlation consistent basis sets for boron through neon. *J. Mol. Struct. THEOCHEM* **388**, 339 (1996).
8. D.E. Woon and T.H. Dunning: Gaussian basis sets for use in correlated molecular calculations. III. The atoms aluminum through argon. *J. Chem. Phys.* **98**, 1358 (1993).
9. S. Miertuš, E. Scrocco and J. Tomasi: Electrostatic interaction of a solute with a continuum. A direct utilizaion of AB initio molecular potentials for the prevision of solvent effects. *Chem. Phys.* **55**, 117 (1981).
10. S. Miertuš and J. Tomasi: Approximate evaluations of the electrostatic free energy and internal energy changes in solution processes. *Chem. Phys.* **65**, 239 (1982).
11. J.L. Pascual-ahuir, E. Silla and I. Tuñon: GEPOL: An improved description of molecular surfaces. III. A new algorithm for the computation of a solvent-excluding surface. *J. Comput. Chem.* **15**, 1127 (1994).
12. R. McWeeny and G. Diercksen: Self-Consistent Perturbation Theory. II. Extension to Open Shells. *J. Chem. Phys.* **49**, 4852 (1968).
13. J.A. Pople and R.K. Nesbet: Self-Consistent Orbitals for Radicals. *J. Chem. Phys.* **22**, 571 (1954).
14. X. Li and M.J. Frisch: Energy-Represented Direct Inversion in the Iterative Subspace within a Hybrid Geometry Optimization Method. *J. Chem. Theory Comput.* **2**, 835 (2006).
15. G. Henkelman, A. Arnaldsson and H. Jónsson: A fast and robust algorithm for Bader decomposition of charge density. *Comput. Mater. Sci.* **36**, 354 (2006).
16. E. Sanville, D. Kenny Steven, R. Smith and G. Henkelman: Improved grid-based algorithm for Bader charge allocation. *J. Comput. Chem.* **28**, 899 (2007).
17. W. Tang, E. Sanville and G. Henkelman: A grid-based Bader analysis algorithm without lattice

bias. *J. Phys.: Condens. Matter* **21**, 084204 (2009).

18. M. Yu and D.R. Trinkle: Accurate and efficient algorithm for Bader charge integration. *J. Chem. Phys.* **134**, 064111 (2011).
19. J. Racine: gnuplot 4.0: a portable interactive plotting utility. *J. Appl. Economet.* **21**, 133 (2006).
20. V. Fock: Näherungsmethode zur Lösung des quantenmechanischen Mehrkörperproblems. *Z. Phys.* **61**, 126 (1930).
21. D.R. Hartree: The Wave Mechanics of an Atom with a Non-Coulomb Central Field. Part I. Theory and Methods. *Math. Proc. Cambridge Philos. Soc.* **24**, 89 (1928).
22. C.C.J. Roothaan: New Developments in Molecular Orbital Theory. *Rev. Mod. Phys.* **23**, 69 (1951).
23. M.J. Frisch, M. Head-Gordon and J.A. Pople: Semi-direct algorithms for the MP2 energy and gradient. *Chem. Phys. Lett.* **166**, 281 (1990).
24. M.J. Frisch, M. Head-Gordon and J.A. Pople: A direct MP2 gradient method. *Chem. Phys. Lett.* **166**, 275 (1990).
25. M. Head-Gordon and T. Head-Gordon: Analytic MP2 frequencies without fifth-order storage. Theory and application to bifurcated hydrogen bonds in the water hexamer. *Chem. Phys. Lett.* **220**, 122 (1994).
26. M. Head-Gordon, J.A. Pople and M.J. Frisch: MP2 energy evaluation by direct methods. *Chem. Phys. Lett.* **153**, 503 (1988).
27. C. Møller and M.S. Plesset: Note on an Approximation Treatment for Many-Electron Systems. *Phys. Rev.* **46**, 618 (1934).
28. S. Sæbø and J. Almlöf: Avoiding the integral storage bottleneck in LCAO calculations of electron correlation. *Chem. Phys. Lett.***154**, 83 (1989).
29. J. Bartlett Rodney and D. Purvis George: Many-body perturbation theory, coupled-pair many-electron theory, and the importance of quadruple excitations for the correlation problem. *Int. J.*

Quantum Chem. **14**, 561 (1978).

30. J. Čížek: On the Use of the Cluster Expansion and the Technique of Diagrams in Calculations of Correlation Effects in Atoms and Molecules. *Adv. Chem. Phys.* (2007).
31. G.D. Purvis and R.J. Bartlett: A full coupled-cluster singles and doubles model: The inclusion of disconnected triples. *J. Chem. Phys.* **76**, 1910 (1982).
32. G.E. Scuseria, C.L. Janssen and H.F. Schaefer: An efficient reformulation of the closed-shell coupled cluster single and double excitation (CCSD) equations. *J. Chem. Phys.* **89**, 7382 (1988).
33. J.P. Perdew, K. Burke and M. Ernzerhof: Generalized Gradient Approximation Made Simple. *Phys. Rev. Lett.* **77**, 3865 (1996).
34. J.P. Perdew, K. Burke and M. Ernzerhof: Generalized Gradient Approximation Made Simple [Phys. Rev. Lett. 77, 3865 (1996)]. *Phys. Rev. Lett.* **78**, 1396 (1997).
35. A.D. Becke: Density-functional thermochemistry. III. The role of exact exchange. *J. Chem. Phys.* **98**, 5648 (1993).
36. C. Lee, W. Yang and R.G. Parr: Development of the Colle-Salvetti correlation-energy formula into a functional of the electron density. *Phys. Rev. B* **37**, 785 (1988).
37. B. Miehlich, A. Savin, H. Stoll and H. Preuss: Results obtained with the correlation energy density functionals of becke and Lee, Yang and Parr. *Chem. Phys. Lett.* **157**, 200 (1989).